# Formation, ripening, and stability of epitaxially strained island arrays

Helen R. Eisenberg* and Daniel Kandel†
*Department of Physics of Complex Systems, Weizmann Institute of Science, Rehovot 76100, Israel*
(Received 20 October 2004; published 23 March 2005)

We study the formation and evolution of coherent islands on lattice-mismatched epitaxially strained films using two-dimensional evolution simulations. Faceted islands form in films with anisotropic surface tension. Under annealing, these islands ripen until a stable array is formed. We show that the presence of a cusp in the surface tension is essential for reproducing the experimentally observed characteristics of the stable island array. It is also shown that a single cusp in the surface energy is sufficient in order to explain the island-shape transition and associated bimodal island-size distribution which occurs in growth experiments. In films with isotropic surface tension we observe and explain a new mode of growth in which a stable wavy surface is formed.

DOI: 10.1103/PhysRevB.71.115423 PACS number(s): 68.55.−a, 81.15.Aa

## I. INTRODUCTION

Coherent (dislocation-free) islands form to relieve the strain associated with lattice-mismatched heteroepitaxial thin films. The islands can then self-organize to create periodic arrays. When such arrays are embedded in a wider band-gap material, they can create quantum dot structures of electronic significance in semiconductor or optoelectronic devices (see, e.g., Ref. 1). Indeed there is currently an explosion of interest (see, e.g., Ref. 2–4) in exploring the use of self-organized quantum dot arrays to create optoelectronic devices, in particular quantum dot lasers.

Of particular interest is whether the island arrays that form are energetically stable or metastable configurations that will ripen. Here we show in annealing simulations that anisotropy in surface tension is necessary for the formation of a stable (roughly periodic) array. Moreover, we show that the presence of a cusp in the surface energy is essential for reproducing the experimentally observed characteristics of the island array, in particular the increase in island density with increasing film thickness.[5–11] The cusped surface tension produces sharply edged faceted islands, which are stabilized by the elastic relaxation the edges contribute. We also show that when surface tension is cusped, islands form in a "chain-reaction ripple" effect (i.e., islands tend to develop near other islands). This mode of growth has also been observed in experiment.[12–14]

Bimodal island-size distributions have been observed experimentally[15–19] and are related to an observed change in the shape of growing islands.[15–19] Due to the relationship between the shape change and the island-size distribution, an understanding of shape transitions is crucial in order to obtain the narrow uniform island size distributions necessary for successful device applications. Previous groups (see, e.g., Ref. 20 and 21) have modeled an island shape transition when two cusped minima are present in the surface tension other than at 0° and hence two distinct faceting angles are present in the crystal shape. We however show that the shape transition and associated bimodal island-size distribution can occur with only one surface tension minimum—that is, without an additional facet orientation at a larger angle.

We see a new phenomenon during long-term annealing after ripening has stopped, in which islands equilibrate to have a very uniform size distribution. We would have to carry out our simulations on larger samples to ensure this is not a finite-size effect. This phenomenon could be very useful in producing uniform quantum dot arrays.

In films with isotropic surface tension we observe and explain a new mode of growth in which a stable wavy surface is formed. Stable, nonflat morphology has previously only been predicted for faceting films.[22–25]

We study the energetic profile of the entire strained island array during film evolution. We consistently see free-energy plateauing during ripening events and then dropping very sharply at the end of the ripening event.

## II. PROBLEM FORMULATION

The self-assembly of quantum dot arrays is not well understood even on the qualitative level. Here, we try to explain the general qualitative behavior observed in typical experimental systems rather than quantitatively reproduce system-specific results. We study the evolution of an elastically isotropic system using continuum theory. The surface of the solid is at $y=h(x,t)$ and the film is in the $y>0$ region with the film-substrate interface at $y=0$. The system is modeled to be invariant in the $z$ direction and hence is essentially two dimensional. This is consistent with plane strain where the solid extends infinitely in the $z$ direction and hence all strains in this direction vanish.[26] All quantities are calculated for a section of unit width in the $z$ direction. The islands we describe are equivalent to elongated island ridges or wires.

All the results mentioned in this paper relate to vicinal surfaces with a very small miscut angle in the $z$ direction. Experimentally, surfaces often have such a small miscut, as it is very difficult to grow a perfect facet.

We assume that surface diffusion is the dominant mass transport mechanism, leading to the following evolution equation [27]:

$$\frac{\partial h}{\partial t} = \frac{D_s \eta \Omega}{k_B T} \frac{\partial}{\partial x} \frac{\partial \mu}{\partial s}, \tag{1}$$

where $D_s$ is the surface diffusion coefficient, $\eta$ is the number of atoms per unit area on the solid surface, $\Omega$ is the atomic

 ©2005 The American Physical Society

volume, $T$ is the temperature, $k_B$ is the Boltzmann constant, $s$ is the arc length, and $\mu$ is the chemical potential at the surface.

In our previous work[28,29] we showed that $\mu$ can be expressed as

$$\frac{\mu}{\Omega} = \tilde{\gamma}(\theta)\kappa + \frac{df_{el}^{(0)}}{dh} + \left(\frac{1}{2}S_{ijkl}\sigma_{ij}\sigma_{kl} - \frac{1}{2}S_{ijkl}\sigma_{ij}^{(0)}\sigma_{kl}^{(0)}\right)\Big|_{y=h(x)}, \tag{2}$$

where $\kappa$ is the surface curvature, $\theta$ is the angle between the normal to the surface and the $y$ direction, and $\tilde{\gamma}(\theta)=\gamma(\theta)+\partial^2\gamma/\partial\theta^2$ is the surface stiffness [with $\gamma(\theta)$ being the surface tension]. $S_{ijkl}$ are the compliance coefficients of the material, $\sigma_{ij}$ is the total stress in the material, $\sigma_{ij}^{(0)}$ is the mismatch stress in the zero-strain reference state, and $f_{el}^{(0)}(h)$ is the reference-state free energy per unit length in the $x$ direction. The reference state is defined as a flat film of thickness $h$ confined to have the lateral lattice constants of the substrate.

Linear stability analysis predicts that a flat film thinner than the linear wetting layer thickness $h_c$ is stable at all perturbation wavelengths and is marginally stable to perturbations of wavelength $\lambda_c$ for thickness $h_c$. The expressions for $h_c$ and $\lambda_c$ are given in Ref. 28 and 29. Above $h_c$ the flat film is unstable to a larger and larger range of wavelengths $\lambda_- \leqslant \lambda \leqslant \lambda_+$ until for infinitely thick films the film is unstable to all perturbations of wavelengths larger than $\lambda=\lambda_c/2$.

We simulated the surface evolution given by Eqs. (1) and (2) and using the numerical scheme described in our earlier work.[29] We used the cusped form of surface tension given by Bonzel and Preuss,[30] which shows faceting in a free crystal: $\gamma(\theta)=\gamma_0[1+\beta|\sin(\pi\theta/(2\theta_0))|]$, where $\beta\approx 0.05$ and $\theta_0$ is the angle of maximum $\gamma$. We considered a crystal which facets at 0°, ±45° and ±90° with $\theta_0=\pi/8$. This is a generic model of crystal surface tension and is only meant to show the general properties of a faceting material and not to correspond exactly to a specific experimental system. The cusp gives rise to $\tilde{\gamma}=\infty$ at the facet angle. However, a slight miscut of the low-index surface along the $z$ direction leads to a rounding of the cusp, which can be described by

$$\gamma(\theta) = \gamma_0\left[1 + \beta\sqrt{\sin^2\left(\frac{\pi}{2\theta_0}\theta\right) + G^{-2}}\right], \tag{3}$$

where $G$ is inversely proportional to the miscut angle and, for example, $G=500$ corresponds to a miscut angle $\Delta\theta \approx 0.1^\circ$ (see Fig. 1 for surface tension plots). As mentioned earlier all the results mentioned in this paper relate to surfaces with a very small miscut angle in the $z$ direction.

$df_{el}^{(0)}(h)/dh$ was obtained from *ab initio* quantum mechanical calculations of $Si_{1-x}Ge_x$ grown on Si(001) (for details see Ref. 33). All our simulations start from a randomly perturbed flat film with an initial thickness denoted by $C$.

## III. RESULTS

When perturbations larger than a critical amplitude [28,29,31] are applied to a flat film, faceted islands develop in the film during both annealing and growth, as illustrated in Fig. 2.

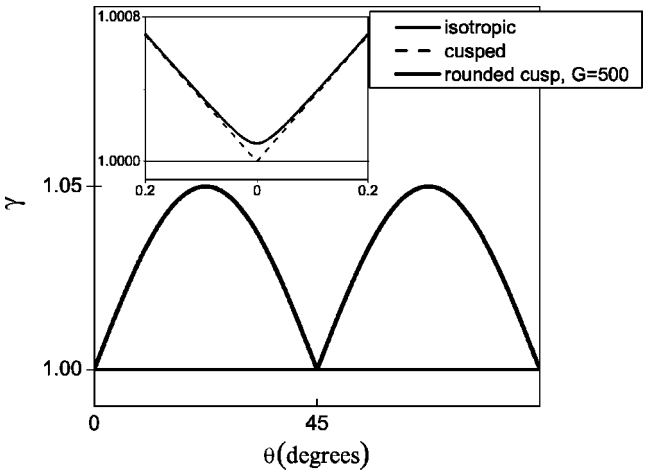


FIG. 1. The figure shows the form of surface tension $\gamma$ used in Eq. (3) and in particular shows the effect of rounding the surface tension cusp. In the isotropic case shown here $\gamma=1$.

The critical perturbation amplitude was largely independent of cusp smoothness $G$, unlike the linear wetting layer thickness which depended strongly on $G$. We carried out most of our simulations for $G=500$ but we also ran selected simulations for $G=5000$ and perfectly cusped surface tension. The results were qualitatively identical and quantitatively very similar. This is important as in experimental systems the exact miscut angle varies and observable phenomena should not be highly dependent on it. The film first becomes unstable at wavelength $\lambda \sim 50\gamma(0)/M\varepsilon^2$, where $M$ is the plain strain modulus and $\varepsilon$ is the lattice mismatch. The islands which form from this perturbation typically have a width of about 10% of the unstable wavelength. Both the unstable wavelength and the faceted island widths scale as $\varepsilon^{-2}$, as observed in experiments[32–35] in which islands develop from long-ripple-like structures (corresponding to our model of plane strain).

All results discussed henceforth refer to Ge/ Si(001) though the same trends were seen in $Ge_{0.5}Si_{0.5}$/Si(001). Islands form in a "chain-reaction ripple" effect (i.e., islands tend to develop near other islands) as is illustrated in Fig. 2. The ripple effect occurs because the growth of the island destabilizes the flat faceted film at its boundaries. This mode of growth has also been observed in experiments.[12–14] Eggleston and Voorhees[36] observed a similar chain reaction of island formation in simulations of a strained film grown on a substrate with a mesa. After initial island formation we observe island ripening occurring over much longer time scales (about 50 times longer).

During annealing the islands are fully faceted. Their tops are faceted at 0° and their sides at 45°. This shape is preserved as the islands grow; i.e., the islands maintain a fixed height-diameter ratio (as seen in experiments[5,15,32,37] and theory[38]). During deposition, on the other hand, an interesting transition is observed in the island shape. Initially, the islands are fully faceted as during annealing. However, when the islands reach a certain diameter, they stop growing laterally and only vertical growth occurs (see Fig. 3). This critical diameter is about 40 nm for Ge islands grown on a Si(001)

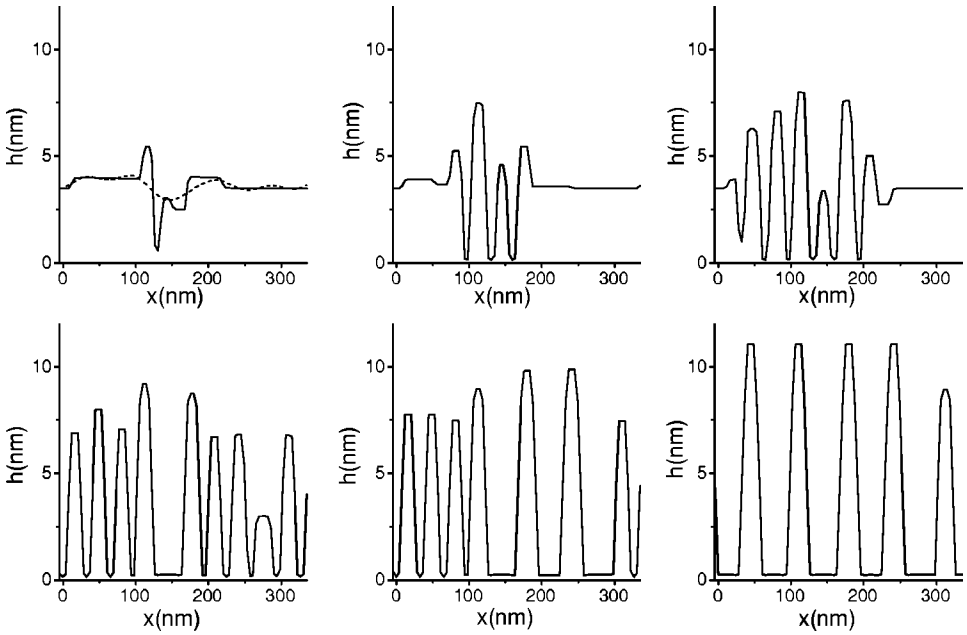


FIG. 2. Evolution of a random perturbation on a 25-monolayer-(ML-) thick Ge film on a Si(001) substrate. In the first graph the dashed line is the initial perturbation and the solid line is the surface at $t=0.028$ s. The second to fifth graphs show the surface at times $t=0.044$ s, 0.068 s, 0.123 s and 2.181 s. The final graph is the stable steady-state island array. Note the ripple effect in island formation and the later island ripening leading to a stable island array. Periodic boundary conditions were applied in the $x$ direction. The same results were observed in simulations with double the period length.

substrate (during annealing we never observed islands which exceeded this diameter). Thus the islands become tall and narrow, and their sides are steeper than 45°. This shape transition is observed experimentally[15,17–19] and is sometimes referred to as the "pyramid-to-dome transition." The driving force behind it is the increased elastic relaxation experienced by tall narrow islands. Theoretical equilibrium calculations with isotropic surface tension[39] show a continuous increase in island aspect ratio with increasing island volume, as elastic effects dominate surface tension effects. The sharp rather than smooth transition in growth mode we observe is due to the anisotropic nature of the surface tension and in particular the presence of a surface tension cusp at 45°. In smaller islands where surface effects dominate, islands are locked into the desired facet angle, until a sharp transition point where the elastic effects dominate and they start growing vertically. Note that contrary to existing explanations of the island shape transition (see, e.g., Refs. 20 and 21), the transition occurs without an additional facet orientation at a larger angle. Altering the exact facet value and/ or having a second steeper faceting angle such as in the dome case, only changes specific quantitative properties of this transition, such as the island size and shape at which the transition occurs.

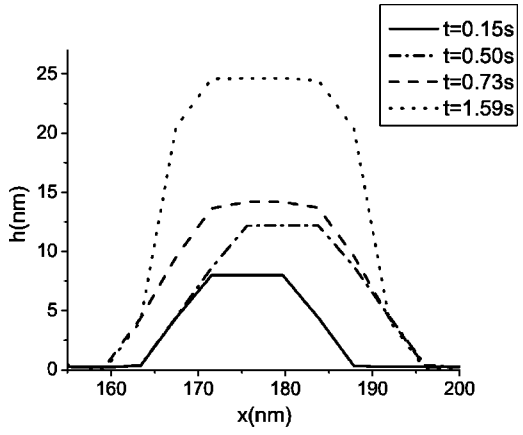


FIG. 3. Island growth during material deposition. In this particular case the island grew in the fixed height-width ratio mode up to $t=0.7$ s and then switched to the vertical growth mode. In this figure Ge was grown on top of a Si(001) substrate. The initial flat film is 10 ML thick and Ge is deposited at a rate of 5.2 nm/s.

The transition in the island-shape and -growth mode is clearly reflected in the size distribution shown in Fig. 4. Narrow island size and spacing distributions are seen during early deposition (see Fig. 4, 20 equivalent monolayers). These narrow distributions are observed in many experiments.[5,6,15–17,19,32,40,41] After additional deposition (30 equivalent monolayers) a *bimodal* distribution forms as some of the islands pass from the fully faceted to the tall narrow shape. At later times (e.g., 50 equivalent monolayers) nearly all islands have the tall narrow shape. At this stage the distribution becomes quite symmetric and evolves at a fixed distribution width (increasing its mean). Similar results were observed in experiments.[15,17–19]

One of our central observations is that annealing of a perturbed flat film with anisotropic surface tension leads to the formation of a stable array of islands. This result is consistent with several experimental systems[7,16,42,43] and is in contrast with films of isotropic surface tension where the islands ripen indefinitely. Theoretical studies also predict stable island arrays.[22–25] The crucial term in determining the stability of an island array apart from anisotropic surface tension and a film-substrate interaction is the presence of an elastic contribution due to island edges. This contribution is automatically present in our calculations and does not need to be introduced separately. Theoretical works that ignore this term[41,44] predict continuous ripening.

Our simulations show that the density of islands in the stable array increases with increasing film thickness (see Fig. 5). An increase in island density with film thickness has also been seen in many experiments.[5–11] Indeed Miller *et al.*[7] and Kamins *et al.*[11] performed annealing experiments and Le-

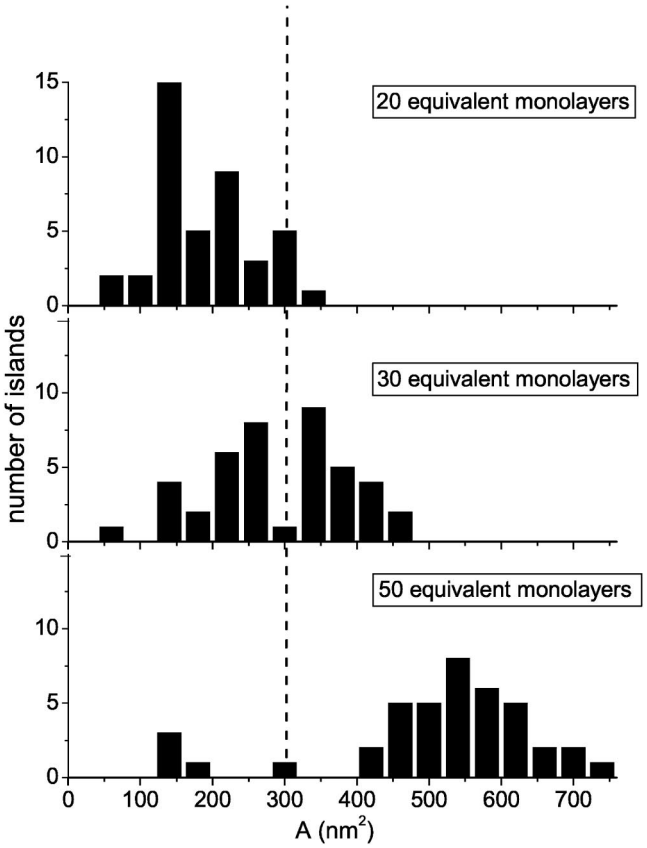


FIG. 4. Distribution of island cross-sectional area $A$ (recall that islands are infinitely long in the $z$ direction), during directed deposition of Ge on a Si(001) substrate. The rate of deposition is 5.2 nm/s, and the initial film height is 10 monolayers. The dashed vertical line shows the separation between the early growth mode in which the island height-width ratio is preserved and the later vertical growth mode.

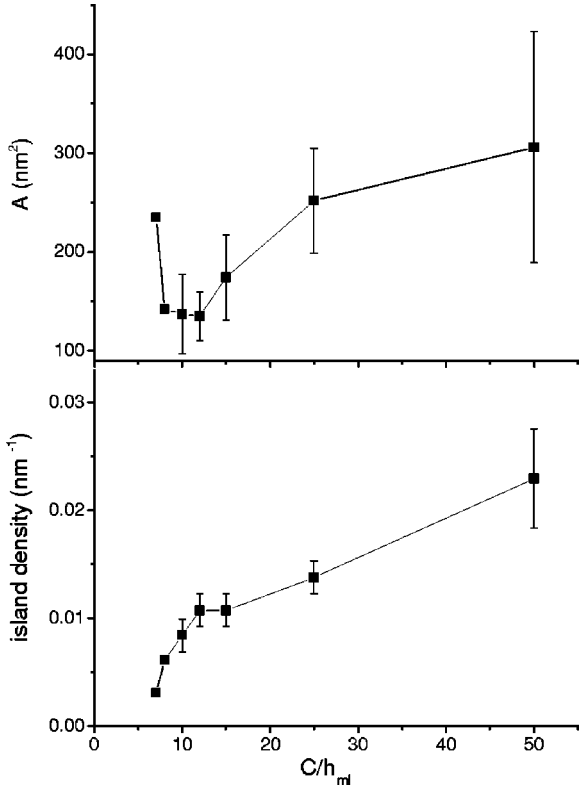


FIG. 5. Island density (bottom graph) and average island cross-sectional area $A$ (top graph) (recall that islands are infinitely long in the $z$ direction), in stable arrays of Ge islands on a Si(001) substrate after ripening has ended. $C$ is the initial flat film thickness, and $h_{ml}$ is the thickness of one monolayer. The error bars refer to the following: Bottom graph: the span of island densities observed with different initial surface morphologies of the same film thickness. Top graph: the standard deviation in island sizes observed throughout all samples of the same film thickness.

onard *et al.*[8] performed experiments with very small deposition rates. These three experiments clearly show the increase in island density as film thickness increases. This result was predicted by Daruka and Barabási[23] in minimal, energy equilibrium calculations. Here we show that the increase in island density also results from evolution simulations. This observation is particularly important, since other evolution studies[22] predicted a decrease in island density with increasing film thickness. We believe this is due to the smooth form of surface tension used in Ref. 22. Indeed, when we carried out simulations with a smooth form of surface tension similar to that used in Ref. 22, we also observed a decrease in island density. This clearly demonstrates the importance of using a cusped form of surface tension to accurately model evolution of faceting surfaces. As we stated earlier the elastic relaxation due to the sharp island edges of faceted islands appears to be critical in order to correctly predict the properties of a faceted island array.

The increase in island density which we observe is an energetic rather than kinetic effect, as the data is obtained from long annealing simulations. Many simulations with different initial surface morphologies but the same flat film thickness have the same final island density, further indicating that this is an equilibrium result.

As can be seen in Fig. 5, the island size also shows a slight increase with increasing film thickness, with islands increasing in width from 25 nm to 40 nm and cross-sectional area from 100 nm$^2$ to 500 nm$^2$ (recall that islands are infinitely long in the $z$ direction). The island size at 7 ML is larger than expected due to finite-size effects. Note that even the smallest islands have a finite nonzero size. Experiments indeed see islands forming only above a certain size which increases with increasing film thickness.[5,6,11,16,41] However, as the annealing experiments which showed stable island arrays tended not to vary the film thickness, it is difficult to compare our results with experimental observations. Our result is in accordance with that predicted in equilibrium calculations by Daruka and Barabási.[23]

The islands in the final island array, during long-term annealing after ripening has stopped, tend to equilibrate so that most islands have exactly the same size apart from occasionally one or two larger or smaller ones (see Figs. 2 and 6). This is unlike the island distribution during evolution or deposition where the size distribution is of finite width (see Figs. 6 and 7). When deposition is halted and the sample annealed, the islands equilibrate so that most have exactly the same size. This is a new effect not seen in other studies.

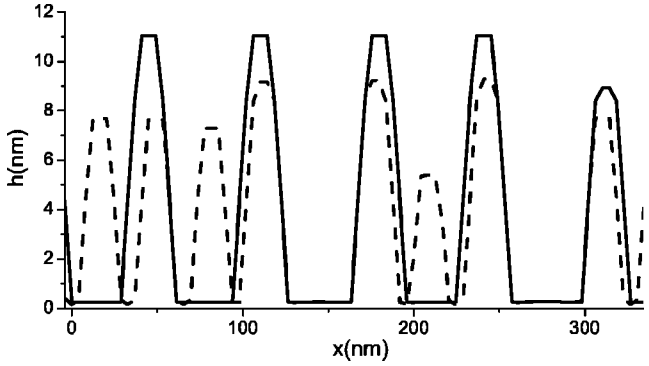


FIG. 6. Surface morphology when a 25-ML film of Ge on a Si(001) substrate is annealed. Periodic boundary conditions were applied in the $x$ direction. The solid line shows the steady-state film after annealing ($t=7.2$ s) the dashed line shows the film during island evolution and ripening ($t=1.5$ s). During evolution the island-size distribution is narrow but finite. In the equilibrium array islands equilibrate so most have exactly the same size.

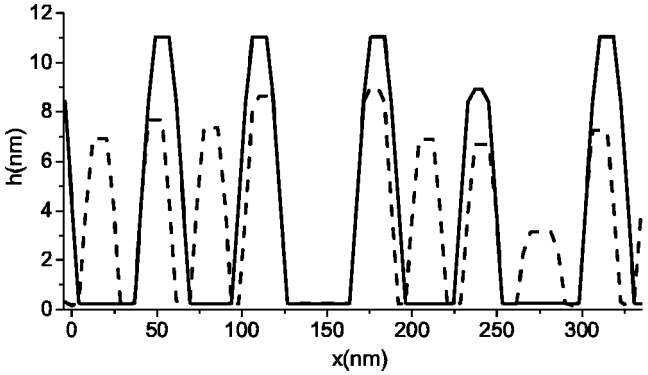


FIG. 7. Surface morphology when Ge is deposited at a rate of 5.2 nm/s onto a 20-ML Ge film on a Si(001) substrate. The dashed line is the surface morphology after 0.14 s of deposition (~5 ML of Ge deposited on top of the 20-ML film). The solid line is the surface morphology after deposition is interrupted and the surface is allowed to equilibrate. During deposition the island-size distribution is narrow but finite. In the equilibrium array islands equilibrate, so most have exactly the same size.

We need to check that this effect also occurs in samples of larger size before we can claim that it is an experimentally observable effect. There do not appear to be any experiments which compare island-size distributions after ripening has stopped during long-time annealing in the absence of dislocated huge islands (Kamins *et al.*[11] who see stable island arrays forming during annealing do compare size distributions but not in the absence of dislocated "superdomes"). This effect could be very useful in producing uniform quantum dot arrays.

When surface tension is isotropic, corresponding to films above the roughening transition temperature, flat film evolution during annealing is very different from that described above. Perturbations in films thinner than $h_c$ decay, and flat films with thickness $h_c<h<h_c+\Delta$, where $\Delta\approx 1$ monolayer, develop a stable smooth wavy morphology at $\lambda_c$. That is, perturbations of other wavelengths decay and perturbations of wavelength $\lambda_c$ grow to a finite amplitude. This is a mode of growth neither seen nor predicted before. Stable, nonflat morphology has previously only been predicted for faceting films.[22–25] In fact, other groups maintain that isotropic films should be unstable to ripening.[22,25,39,45] While films are linearly unstable to perturbations of wavelengths $\lambda_-\leqslant\lambda\leqslant\lambda_+$, our simulations show that the nonlinearity stabilizes the growth of wavelengths close to $\lambda_-$ and $\lambda_+$. As a result the

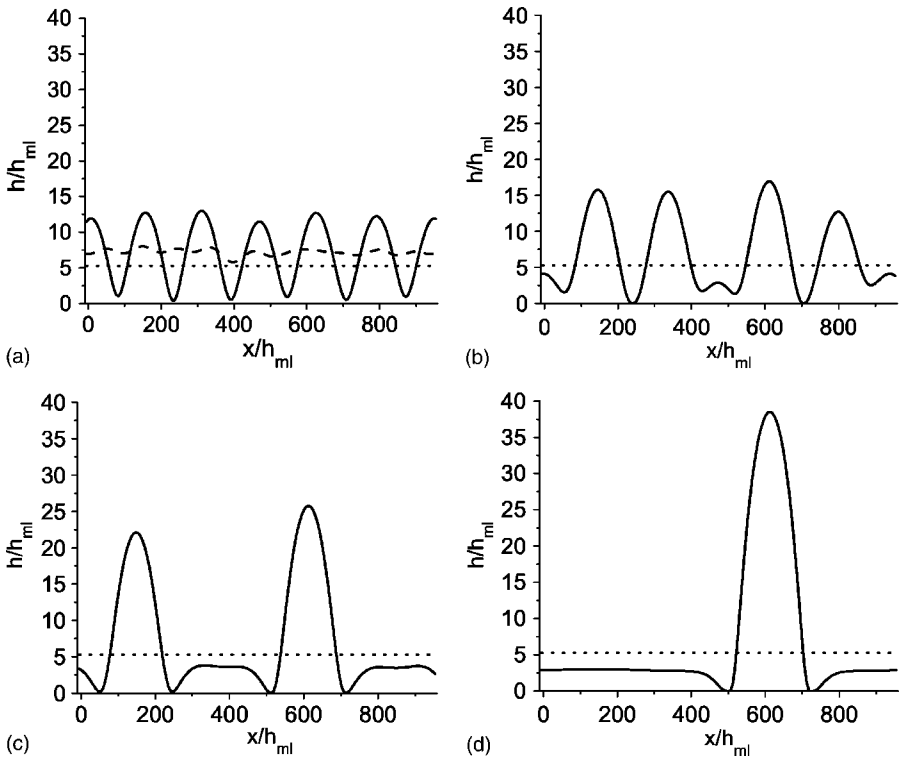


FIG. 8. Evolution of a random perturbation on an isotropic film of height $C=7.2$ ML$=h_c+1.9$ ML. $\varepsilon=2\%$. The dotted line represents the linear wetting layer thickness. In the first graph, the dashed line represents the initial randomly perturbed film and the solid line the surface at $t=4$s. The second graph shows the surface at $t=40$ s, the third at $t=96$s and the last graph the surface at $t=255$ s. $h_{ml}$ is the thickness of one monolayer.

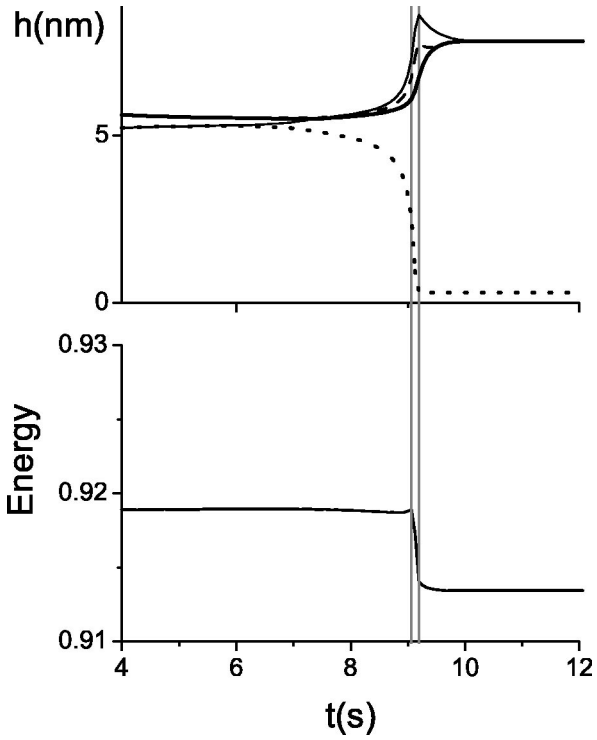


FIG. 9. Top graph: evolution of island peaks when 10 ML of Ge is annealed on a Si(001) surface. Four long-living islands have developed by 0.1 s. Peak 1 is represented by a thick black line peak 2 by a thin black line, peak 3 by a dotted line, and peak 4 by a dashed line. As can be seen a ripening event occurs in which peak 3 disappears. Bottom graph: the free energy as the system evolves. Note that the free energy plateaued during the ripening event and only dropped sharply at the very end of the ripening event. The energy is given in relation to the free energy of a flat film of 10 ML.

growth of the perturbation saturates and stops at a finite amplitude, as seen by Spencer and Meiron[46] for infinitely thick films. When films are sufficiently close to the linear wetting layer thickness, the range of nonlinear saturation extends over the entire range of linearly unstable wavelengths and so a stable wavy morphology is observed. For films thicker than $h_c+\Delta$, initially a wavy structure at the most unstable wavelength forms. The hills of these waves then ripen on larger and larger length scales, until isolated islands are left that continue ripening (see Fig. 8).

In all our simulations we saw several common aspects to the ripened morphology which we also observed in films with faceted islands, suggesting that these features arise due to the interplay between relieving the linear elastic strain energy and the nonlinear elastic energy (the wetting layer term) and are independent of the form of the surface tension. These features were also observed in many experiments. All of them can be observed in the well separated island morphologies during the later evolution in Fig. 8. The linear wetting layer disappears once islands begin to form and a new thinner flat wetting layer of 2–3 ML remains between the islands (observed in experiments in Refs. 32, 33, 37, and 42). Note the inter island wetting layer thickness was the same independent of lattice mismatch unlike other morphological features such as island size. This is because it is the

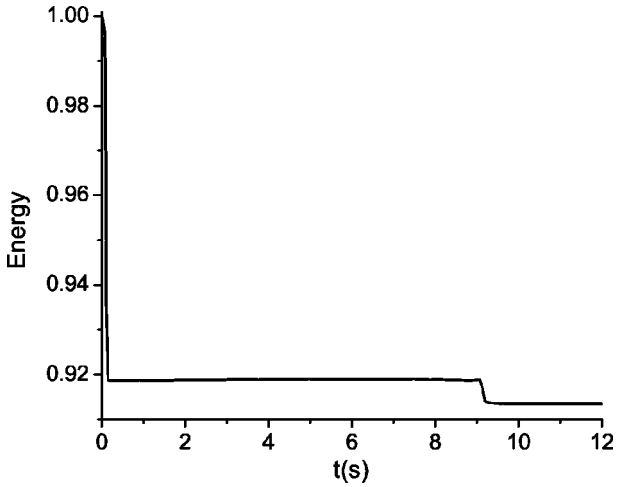


FIG. 10. Free energy over the entire simulation time range. Note the sharp energy drop during faceting and the ripening energy plateau.

decay length of $df_{el}^{(0)}/dh$ which governs behavior very near to the interface and this is independent of lattice mismatch. A depression around the base of the islands is observed (experimental evidence in Ref. 15 and 32, also seen in simulations[22]).

## IV. ENERGY CALCULATIONS

We calculated the total free energy [Eq. (4)] of the film-substrate system for particular surface profiles, in order to measure how the free energy changes during ripening events.

The free energy of the whole substrate-film system is given by

$$F = F_{el} + \int dx \gamma \sqrt{1 + (\partial h/\partial x)^2}, \tag{4}$$

where $F_{el}$ is the elastic free energy including any elastic contributions to the surface tension:

$$F_{el} = \int dx f_{el}^{(0)} + \int dx \int_{-\infty}^{h(x)} dy \left( \frac{1}{2} S_{ijkl} \sigma_{ij} \sigma_{kl} - \frac{1}{2} S_{ijkl} \sigma_{ij}^{(0)} \sigma_{kl}^{(0)} \right) \tag{5}$$

In order to calculate the stresses at the surface we solved a boundary integral equation in terms of the complex Goursat functions, the details of which can be found in the paper of Spencer and Meiron.[46]. The stress throughout the solid was then determined by utilizing the fact that the Goursat functions are analytical in the solid region and using the Cauchy integral formula.

Consistently for both isotropic and anisotropic surface tension the free energy plateaued during the ripening event and only dropped sharply at the very end of the ripening event. For example, see Figs. 9–11, which show how the total free energy and film morphology change when an island disappears during a ripening event in a Ge film on a Si(001) substrate. For anisotropic surface tension there was a very sharp drop in energy during initial faceting and island formation.

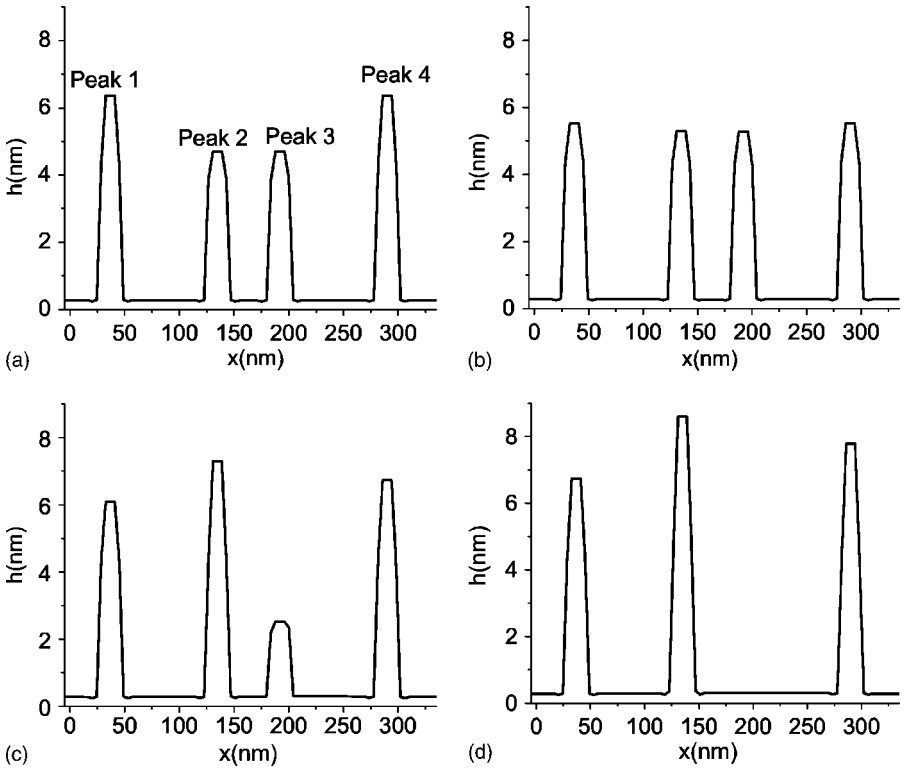


FIG. 11. Evolution of island peaks when 10 ML of Ge is annealed on a Si(001) surface. (a) $t=0.15$ s. Four long-living faceted islands have now fully developed. The energy has plummeted from the energy of the initial perturbed flat film corresponding to the highly energetically favorable process of faceted island formation. Energy now plateaus while small changes in relative island height takes place. (b) $t=5.98$ s The middle of the energy plateau and the beginning of the ripening process in which peak 3 will disappear. From now on the other peaks will grow at peak 3's expense. (c) $t=9.06$s. The start of the drop in the energy plateau, corresponding to the first vertical line in Fig. 9. The morphological ripening is, however, very advanced and peak 3 is much smaller than the other peaks. (d) $t=9.20$ s. The end of the ripening event, corresponding to the second vertical line in Fig. 9. Note that the big energy drop takes place only at the end of the ripening event.

## V. SUMMARY

Like other groups before us[22,25] we show that surface tension anisotropy is crucial to the formation of stable island arrays and the prevention of continuous ripening. However, the type of anisotropy used in these previous works[22,25] was smooth and not cusped and hence did not lead to faceting. As we show, having cusped surface tension is crucial in correctly determining the characteristics of the island array, in particular in showing an increasing rather than decreasing island density with increasing film thickness. The cusped surface tension is essential in producing sharply edged faceted islands and therefore the stabilizing elastic relaxation these island edges contribute. We also show that when surface tension is cusped islands form in a "chain-reaction ripple" effect (i.e., islands tend to develop near other islands). This mode of growth has also been observed in experiment.[12–14]

We see a new phenomenon during long-term annealing after ripening has stopped, in which islands equilibrate to have a very uniform size distribution. We would have to carry out our simulations over larger samples to ensure this is a nonlocal effect. There do not appear to be any experiments which compare island-size distributions after ripening has stopped during long-time annealing in the absence of dislocated huge islands. This could be very useful in producing uniform quantum dot arrays.

We show that the island-shape transition can occur with only one surface tension minimum—that is, without an additional facet orientation at a larger angle.

In films with isotropic surface tension we observe and explain a new mode of growth in which a stable wavy surface is formed. Stable, nonflat morphology has previously only been predicted for faceting films.[22–25] Experiments above the roughening temperature would need to be carried out to verify our prediction.

We studied the energetic profile of the entire strained island array during film evolution. We consistently see free-energy plateauing during ripening events and then dropping very sharply at the end of the ripening event.

## APPENDIX

In this appendix we calculate expressions for the strain energy of a perturbed uniaxially and biaxially strained film. As these calculations show, the two expressions differ only by a constant dependent only on the mismatch strain and independent of the surface morphology. This leads only to a change in energy and length scales (due to the differing mismatch stress) but not in the qualitative features of the observed phenomena.

We use the following definition of strain:

$$e_{ij} = \frac{1}{2}\left(\frac{\partial u_i}{\partial x_j} + \frac{\partial u_j}{\partial x_i}\right),$$

where $u$ are material displacements. The shear modulus is $\mu = E/2(1+\nu)$, where $E$ is Young's modulus and $\nu$ is Poisson's ratio.

The stress-strain relations are then

$$e_{ij} = \frac{1}{E}[(1+\nu)(\sigma_{ij} - \sigma_{ij}^{(0)}) - \nu(\sigma_{kk} - \sigma_{kk}^{(0)})\delta_{ij}], \quad \text{(A1)}$$

where $\sigma$ is the total stress in the material and $\sigma^{(0)}$ is the stress in the zero-strain reference state.

From the above expression we obtain the compliance coefficients $S_{ijkl}[e_{ij} = S_{ijkl}(\sigma_{kl} - \sigma_{kl}^{(0)})]$. The elastic free-energy density can be written as

$$f_v = f_v^{(0)} + \frac{1}{2}S_{ijkl}\sigma_{ij}\sigma_{kl} - \frac{1}{2}S_{ijkl}\sigma_{ij}^{(0)}\sigma_{kl}^{(0)}, \quad \text{(A2)}$$

where $f_v^{(0)}$ is the free-energy density in the zero-strain reference state.

### Uniaxial strained film

The plane strain conditions are $e_{zz} = e_{xz} = e_{yz} = 0$.

Using the stress-strain relations (A1) these conditions can be rewritten in terms of stresses: $\sigma_{zz} - \sigma_{zz}^{(0)} = \nu[(\sigma_{xx} - \sigma_{xx}^{(0)}) + (\sigma_{yy} - \sigma_{yy}^{(0)})]$, $\sigma_{xz} = \sigma_{xz}^{(0)}$, and $\sigma_{yz} = \sigma_{yz}^{(0)}$.

Substituting for $\sigma_{zz}$, $\sigma_{xz}$, and $\sigma_{yz}$, in Eq. (A2) and explicitly writing the compliance coefficients, we obtain

$$f_v = f_v^{(0)} + \frac{1+\nu}{2E}\{(1-\nu)(\sigma_{xx}^2 + \sigma_{yy}^2) - 2\nu\sigma_{xx}\sigma_{yy} + 2\sigma_{xy}^2 - (1-\nu)$$
$$\times[(\sigma_{xx}^{(0)})^2 + (\sigma_{yy}^{(0)})^2] + 2\nu\sigma_{xx}^{(0)}\sigma_{yy}^{(0)} - 2(\sigma_{xy}^{(0)})^2\}. \quad \text{(A3)}$$

We are interested in the free-energy density $f_v$ at the surface and hence can use the zero-force surface boundary conditions, which yield

$$n_x\sigma_{xx} + n_y\sigma_{xy} = 0,$$

$$n_x\sigma_{xy} + n_y\sigma_{yy} = 0,$$

where **n** is the normal to the surface. The same conditions also apply separately to the reference state stresses.

Combining the two boundary condition equations above leads to the following relation between the stress components at the surface:

$$\sigma_{xx}\sigma_{yy} = \sigma_{xy}^2.$$

Inserting this relation into the expression for the elastic free-energy density, Eq. (A3), gives a much simplified expression for the free-energy density at the surface:

$$f_v = f_v^{(0)} + (\sigma_{xx} + \sigma_{yy})^2/(2M) - (\sigma_{xx}^{(0)} + \sigma_{yy}^{(0)})^2/(2M),$$

where $M = E/(1-\nu^2)$ is the plane strain modulus. The mismatch stress in a uniaxially strained film is given by $\sigma_{xx}^{(0)} = M\varepsilon$.

### Biaxially strained film

In the case of biaxial strain, $e_{xz} = e_{yz} = 0$, $e_{zz} = \varepsilon$, and $\sigma_{zz} - \sigma_{zz}^{(0)} = \nu(\sigma_{xx} - \sigma_{xx}^{(0)} + \sigma_{yy} - \sigma_{yy}^{(0)}) + E\varepsilon$. Hence,

$$f_v = f_v(\text{plane strain}) + E\varepsilon^2/2 + [\sigma_{zz}^{(0)} - \nu(\sigma_{xx}^{(0)} + \sigma_{yy}^{(0)})]\varepsilon.$$

The mismatch stress in a biaxially strained film is given by $\sigma_{xx}^{(0)} = \sigma_{zz}^{(0)} = [E/(1-\nu)]\varepsilon = M(1+\nu)\varepsilon$. Hence the free energy under biaxial stress differs from that in plane strain by a constant which has no effect on the morphological evolution of the surface.

The increase in mismatch stress in the biaxial case just has the effect of changing energy and length scales. The evolution equations [Eq. (1) together with Eq. (2)] can be made spatially dimensionless by scaling all lengths by $l_0 = \gamma_0/S_0$ where $\gamma_0$ is the surface tension of the flat film and $S_0$ is the elastic energy density of the flat film, and all times by $\tau = \gamma_0^3 k_B T/D_s\eta\Omega^2 S_0^4$. The strain energy density is scaled by $S_0$. Note that $df_{el}^{(0)}/dh$ can be written as $S_0 f'(h/h_{ml})$ where $f'(h/h_{ml}) \to 1$ as $h \to \infty$. Hence

$$\frac{\partial h}{\partial t} = \frac{D_s\eta\Omega^2}{k_B T}\frac{\partial}{\partial x}\frac{\partial[\tilde{\gamma}\kappa + S + S_0 f'(h/h_{ml})]}{\partial s}, \quad \text{(A4)}$$

becomes

$$\frac{\partial\tilde{h}}{\partial\tilde{t}} = \frac{\partial}{\partial\tilde{x}}\frac{\partial[\tilde{\gamma}\tilde{\kappa} + \tilde{S} + f'(\tilde{h}/\tilde{h}_{ml})]}{\partial\tilde{s}}, \quad \text{(A5)}$$

where all variables are written in terms of the scaled variables and are represented by a tilda above the original symbols.

Hence having a finite rather than zero strain in the $z$ direction does not change any qualitative features of our results.

*Electronic address: helen@engineering.ucsb.edu

†Present address: KLA-Tencor Corporation (Israel), 4 Hatikshoret St., Migdal-Haemek, Israel.

[1] D. L. Huffaker, G. Park, Z. Zou, O. B. Shchekin, and D. G. Deppe, Appl. Phys. Lett. **73**, 2564 (1998).

[2] P. Bhattacharya and S. Ghosh, Appl. Phys. Lett. **80**, 3482 (2002).

[3] M. Sugawara, N. Hatori, T. Akiyama, Y. Nakata, and H. Ishikawa, Jpn. J. Appl. Phys., Part 2 **40**, L488 (2001).

[4] R. L. Sellin, Ch. Ribbat, M. Grundmann, N. N. Ledenstov, and D. Bimburg, Appl. Phys. Lett. **78**, 1207 (2001).

[5] Y.-W Mo, D. E. Savage, B. S Swartzentruber, and M. G Lagally, Phys. Rev. Lett. **65**, 1020 (1990).

[6] M. Kastner and B. Voigtlander, Phys. Rev. Lett. **82**, 2745 (1999).

[7] M. S. Miller, S. Jeppesen, D. Hessman, B. Kowalski, I. Maximov, B. Junno, and L. Samuelson, Solid-State Electron. **40**, 609 (1996).

[8] D. Leonard, K. Pond, and P. M. Petroff, Phys. Rev. B **50**, 11 687 (1994).
[9] T. R. Ramachandran, R. Heitz, P. Chen, and A. Madhukar, Appl. Phys. Lett. **70**, 640 (1997).
[10] N. P. Kobayashi, T. R. Ramachandran, P. Chen, and A. Madhukar, Appl. Phys. Lett. **68**, 3299 (1996).
[11] T. I. Kamins, G. Medeiros-Ribeiro, D. A. A. Ohlberg, and R. Stanley Williams, J. R. Astron. Soc. Can. **85**, 1159 (1999).
[12] R. M Tromp, F. M. Ross, and M. C Reuter, Phys. Rev. Lett. **84**, 4641 (2000).
[13] P. Sutter and M. G. Lagally, Phys. Rev. Lett. **84**, 4637 (2000).
[14] D. E. Jesson, K. M. Chen, S. J Pennycook, T. Thundat, and R. J. Warmack, Phys. Rev. Lett. **77**, 1330 (1996).
[15] T. I. Kamins, E. C. Carr, R. S. Williams, and S. J. Rosner, J. Appl. Phys. **81**, 211 (1997).
[16] G. Medeiros-Ribeiro, T. I. Kamins, D. A.A. Ohlberg, and R. S. Williams, Phys. Rev. B **58**, 3533 (1998).
[17] F. M. Ross, J. Tersoff, and R. M. Tromp, Phys. Rev. Lett. **80**, 984 (1998).
[18] A. Rastelli and H. von Känel, Surf. Sci. Lett. **515**, L493 (2002).
[19] N. V. Vostokov *et al.*, J. Cryst. Growth **209**, 302 (2000).
[20] Y. W. Zhang and A. F. Bower, Appl. Phys. Lett. **78**, 2706 (2001).
[21] I. Daruka, J. Tersoff, and A.-L. Barabási, Phys. Rev. Lett. **82**, 2753 (1999).
[22] C.-h. Chiu, Appl. Phys. Lett. **75**, 3473 (1999).
[23] I. Daruka and A.-L. Barabási, Phys. Rev. Lett. **79**, 3708 (1997).
[24] V. A. Shchukin, N. N. Ledentsov, P. S. Kop'ev, and D. Bimberg, Phys. Rev. Lett. **75**, 2968 (1995).
[25] Y. W. Zhang, Phys. Rev. B **61**, 10 388 (2000).
[26] Actually experimental systems are generally under biaxial stress, and so for a *z*-direction-invariant model all shear strains in that direction would vanish ($e_{xz}=e_{yz}=0$) and the misfit tensile strain would be constant ($e_{zz}=\varepsilon$). However, as we show in the Appendix, a finite (rather than zero) value of strain in the *z* direction only modifies the equations of elasticity by a constant. This only leads to a change in energy and length scales but not in the qualitative features of the observed phenomena.
[27] W. W. Mullins, J. Appl. Phys. **28**, 333 (1957).
[28] H. R Eisenberg and D. Kandel, Phys. Rev. Lett. **85**, 1286 (2000).
[29] H. R Eisenberg and D. Kandel, Phys. Rev. B **66**, 155429 (2002).
[30] H. P. Bonzel and E. Preuss, Surf. Sci. **336**, 209 (1995).
[31] H. R Eisenberg, D. Kandel, E. Kaxiras, and I. N. Remediaki (unpublished).
[32] J. A Floro, E. Chason, R. D. Twesten, R. Q. Hwang, and L. B. Freund, Phys. Rev. Lett. **79**, 3946 (1997);J. A. Floro, E. Chason, L. B Freund, R. D Twesten, R. Q. Hwang, and G. A Lucadamo, Phys. Rev. B **59**, 1990 (1999).
[33] W. Dorsch, B. Steiner, M. Albrecht, H. P Strunk, H. Wawra, and G. Wagner, J. Cryst. Growth **183**, 305 (1998).
[34] A. J. Pidduck, D. J. Robbins, A. G. Cullis, W. Y. Leong, and A. M. Pitt, Thin Solid Films **222**, 78 (1992).
[35] B. H. Koo, T. Hanada, H. Makino, and T. Yao, Appl. Phys. Lett. **79**, 4331 (2001).
[36] J. J. Eggleston and P. W. Voorhees, Appl. Phys. Lett. **80**, 306 (2002).
[37] J. M. Moison, F. Houzay L. Leprince, E. andre, and O. Vatel, Appl. Phys. Lett. **64**, 196 (1994).
[38] F. Long, S. P.A. Gill, and A. C.F. Cocks, Phys. Rev. B **64**, 121307 (2001).
[39] B. J. Spencer and J. Tersoff, Phys. Rev. Lett. **79**, 4858 (1997).
[40] D. E. Jesson, G. Chen, K. M. Chen, and S. J. Pennycook, Phys. Rev. Lett. **80**, 5156 (1998).
[41] J. A. Floro, G. A. Lucadamo, E. Chason, L. B. Freund, M. Sinclair, R. D. Twesten, and R. Q. Hwang, Phys. Rev. Lett. **80**, 4717 (1998);J. A. Floro, M. B. Sinclair, E. Chason, L. B. Freund, R. D. Twesten, R. Q. Hwang, and G. A. Lucadamo, *ibid.* **84**, 701 (2000).
[42] C. S. Ozkan, W. D. Nix, and H. Gao, Appl. Phys. Lett. **70**, 2247 (1997).
[43] G. E. Cirlin, G. M. Guryanov, A. O. Golubok, S. Ya. Tipissev, N. N. Ledentsov, P. S. Kop'ev, M. Grundmann, and D. Bimberg, Appl. Phys. Lett. **67**, 97 (1995).
[44] J. Tersoff, and F. K. LeGoues, Phys. Rev. Lett. **72**, 3570 (1994).
[45] R. V. Kukta, and L. B. Freund, J. Mech. Phys. Solids **45**, 1835 (1997).
[46] B. J. Spencer, and D. I. Meiron, Acta Metall. Mater. **42**, 3629 (1994).